Applied Thermal Engineering 147 (2019) 1096–1106

Contents lists available at ScienceDirect

Applied Thermal Engineering

journal homepage: www.elsevier.com/locate/apthermeng

Research Paper

Thermal performances of a multi-scale fluidic network

Cyril Pistoresi, Yilin Fan, Julien Aubril, Lingai Luo*

Laboratoire de Thermique et Energie de Nantes, UMR CNRS 6607, Polytech' Nantes – Université de Nantes, La Chantrerie, Rue Christian Pauc, BP 50609, 44306 Nantes Cedex 03, France

HIGHLIGHTS

- Thermal performances of a multi-scale structured fluidic network.
- Design and develop globally macro-sized, locally micro-structured process equipment.
- Cooling performance of a single plate heat sink embodying the multi-scale network.
- Novel plate heat exchanger comprising of a number of multi-scale structured plates.

GRAPHICAL ABSTRACT

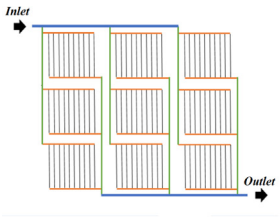

Multi-scale fluidic network

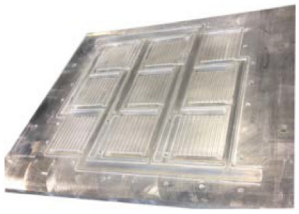

Single-plate multi-scale structured heat sink

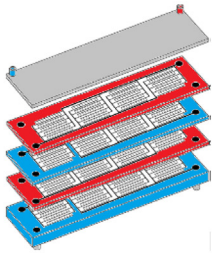

Novel concept of plate-type heat exchanger

ARTICLE INFO

Keywords:
Multi-scale
Fluidic network
Thermal performance
Heat sink
Plate heat exchanger

ABSTRACT

This paper presents an original study on the heat transfer characteristics of a multi-scale structured fluidic network consisting of a number of minichannels in parallel. Two sets of application are tested, including a single plate heat sink being heated on its base surface and a two-stream plate-type heat exchanger when several such plates are stacked one above another. Computational Fluid Dynamics (CFD) simulations were performed to characterize local temperature profiles and thermal performances in such a complex geometry. In parallel, a prototype made of Aluminum was fabricated and tested, providing experimental results for comparison and validation of the obtained numerical results.

Results indicate that when used as a heat sink for cooling purpose, the overall thermal resistances of the multi-scale structuration concept are remarkably smaller than some micro- or mini-channels heat sinks tested in the literature. When used as a novel two-fluid plate-type heat exchanger, the volumetric heat transfer power could reach about 25 MW m^{-3}. This novel concept of multi-scale structured plate heat exchanger showcases how to design and develop globally macro-sized, locally micro (milli)-structured process equipment while keeping high performances, aiming at large-scale industrial applications.

1. Introduction

The process engineering and chemical industries are undergoing a drastic change, facing more and more important energy and environment issues for our society. Process Intensification (PI) brings "paradigm shift" to process design, proposing smaller, less costly, cleaner, safer, higher productivity and more energy efficient processes [1]. One of the routes to realize PI is through miniaturization, more precisely the employment of microstructured technologies, providing a high surface-to-volume ratio, hence enhancing mass and heat transfer [2].

In this context, many ultra-compact heat exchangers have been developed and applied in various fields including medical, energy, biological and chemical processes, as summarized by many of the review papers e.g., [3–5]. However, PI by augmentation of the surface to

* Corresponding author.
E-mail address: lingai.luo@univ-nantes.fr (L. Luo).

https://doi.org/10.1016/j.applthermaleng.2018.11.015
Received 1 May 2018; Received in revised form 18 September 2018; Accepted 4 November 2018
Available online 07 November 2018
1359-4311/

Nomenclature

AR	aspect ratio
C_p	specific heat [J kg^{-1} K^{-1}]
D	pumping power consumption [W]
D_h	channel hydraulic diameter [m]
e	thickness [m]
H	global heat transfer coefficient [W m^{-2} K^{-1}]
L	length [m]
m	mass flow-rate [kg s^{-1}]
q_w	heat flux [W m^{-2}]
Re	Reynolds number [–]
R_{th}	global thermal resistance [K W^{-1}]
S	heat transfer surface area [m^2]
T	temperature [K]
U	overall heat transfer coefficient [W m^{-2} K^{-1}]
v	viscosity [Pa s]
W	width [m]

Greek symbols

Δp	pressure loss [Pa]
ΔT_{LMTD}	temperature difference based on LMTD method [K]
ρ	density [kg m^{-3}]
λ	thermal conductivity [W m^{-1} K^{-1}]
Φ	heat transfer rate [W]

Subscripts

ch	channel
f	fluid
max	maximum
w	solid part

volume ratio also has its limits [6]: vulnerable to fouling, clogging and flow maldistribution, fragile to corrosion, high pressure drop and high fabrication cost. In fact, the manufacturing tolerances, the surface quality and roughness become much more difficult to handle when the channel characteristic dimension decreases to a certain level, causing negative influences on the flow behavior as well as on the process [7]. Therefore for certain aimed application and operational conditions, a compromise on the channel dimension may have to be reached between the advantages of micro-structure and the above-mentioned influencing factors.

Moreover, the parallelization of multiple channels is often necessary to achieve high throughput for industrial application. A well-acknowledged approach is the so-called equaling-up concept [3,8] that is to increase the channel dimension (scaling-up) to a point where still high performances of micro-structure can be obtained, and then to parallelize (numbering-up). This concerns the design and developement of globally macro-sized, locally micro (milli)-structured process equipment while keeping enhanced, controllable and reproducible process performances. The multi-scale approach then makes it possible by bridging the local micro-scale to the overall macro-scale via several intermediate meso-scales.

Besides the tree-like arborescence based on dichotomic or tetratomic ramification, the “ladder-type” or “comb-type” structure as a typical multi-scale fluidic network is also receiving increasing attention, which can be subsumed under a more general notion as “vascularization with trees matched canopy-to-canopy” proposed by Bejan and coworkers e.g., [9,10]. While most of the early work is concerned with simple architectures (simple Z-ladders), in which a bunch of parallel tubes or channels is connected to a perpendicular distributing tube and a collecting tube (e.g., shown in [11] or [12]), recent works consider more complex networks involving several scales with intermediate connections and different geometric variations (e.g., shown in [13]). All these scales are characterized by their own dominant mechanisms; they behave mostly independently, but subject, to some extent, to the constraints of the others.

One of the interesting applications of such ladder-type networks is the cooling of a heat generating surface or volume, i.e., being used as a heat sink. Many efforts have been devoted to assessing the fluid flow and heat transfer characteristics for the purpose of improving their cooling performances. For elementary Z-ladder, Lu and Wang [14] and Chein and Chen [15] numerically investigated the effect of inlet and/or outlet positions on the temperature distribution non-uniformity of the microchannel heat sink surface. Based on their analytical work, Saber et al. [16] reported that the thermal efficiency of the Z-ladder decreased with the increasing number of micro-channels, mainly because of the presence of higher flow distribution non-uniformity. Cho et al. [17] experimentally tested the cooling performances of microchannel Z-type heat sinks under uniform and non-uniform heat flux conditions. They reported that the diverging channel with a trapezoidal header was their best combination considering the temperature distribution and pressure drop. A gas-to-gas micro heat exchanger with double layers of Z-ladder network stacked one above another were proposed and tested in KIT, Germany [18,19]. It has been emphasized that the fluid-dynamic design of the manifolds is of primary importance for the performance optimization. Solovitz et al. [20] proposed to vary the size of parallel microchannels so as to reach an equal nondimensional temperature among all channels. Mu et al. [21] found that the temperature non-uniformity on the heating surface and the global thermal resistance of a mini-channels heat sink could be decreased by varying the channel height (thus the aspect ratio) along the flow direction and using circular turning type distributor. Shen et al. [22] studied the double-layered microchannel heat sinks and optimized the height ratio of two layers and the length of the upper layer. A wavy configuration between two layers in staggered arrangement was also proposed and tested [23]. Soleimanikutanaei et al. [24] numerically studied the heat transfer enhancement through the use of transverse microchannels (Z-type ladder) in a heat sink. Other studies focused on adding inserts with different shapes (e.g., Y-shape [25]; I-shape [26], etc.) or structured metal foams [27,28] inside the parallel microchannels to further enhance the heat transfer.

Relatively fewer studies have focused on the thermal performances of a multi-scale structured fluidic network having a parallel arrangement of elementary Z-ladders. Saber et al. [16] found that arranging the flows in different ways yields different hydrothermal characteristics. A compromise between flow distribution uniformity, small pumping power consumption and efficient heat transfer can be attained by increasing the structure complexity inside the heat exchanger. Cho et al. [29] and Cho and Kim [30] conducted both numerical and experimental investigations on the cooling performance of similar multi-scale (vascularized) structures. They reported that the optimization of vascular channel constructs could lead to much lower flow resistance and more uniform temperature distribution. Multi-scale multichannel devices, also named as Self-Similarity Heat Sinks (SSHS) with a multi-scale arrangement of complex micro-structures have been proposed and investigated [31–34]. High heat removal capacity (heat flux up to 1000 W cm^{-2}) could be achieved. More degrees of freedom may be obtained by proposing sandwich-type heat sinks cored with different metallic lattices, i.e. X-shape [35], pyramidal-shape [36] or Kagome-shape [37]. High overall heat removal capacity has been reported.

In our previous work [38], the fluid flow characteristics of a multi-scale fluidic network consisting of 9 elementary Z-ladders and 90 parallel mini-channels have been investigated and discussed. A special effort was made to improve the flow distribution uniformity by

inserting the geometrically optimized perforated baffles [39,40], which has been proved to be really cost-effective. As the following of [38], this paper presents the thermal performances of such multi-scale structured fluidic network so as to illustrate the benefits of multi-scale structuration concept. Since an analytical description of the flow remains elusive due to the non-developed flow patterns in such a complex geometry, a numerical study is performed to provide an insight of the thermal-fluid characteristics. The main objectives and originalities of the paper are then twofold: (1) to investigate heat transfer characteristics of the network used as a heat sink to remove the heat absorbed at its base surface, using appropriate numerical and experimental techniques; and (2) to assess the global thermal performance of a two-fluid plate heat exchanger comprising of a number of multi-scale structured plates stacked one above another.

The rest of the paper is organized as follows. Section 2 describes the prototype of the multi-scale fluidic network tested in this study. Section 3 presents the used methodologies including the Computational Fluid Dynamics (CFD) simulation parameters and the experimental set-up. Section 4 presents and discusses the results obtained. Finally in Section 5, main findings of this study as well as the future research directions are summarized.

2. Geometry and device

The studied geometry of multi-scale network is exactly the same as that shown in Fig. 1 of [38], with 90 mini-channels in total. Ten identical mini-channels are arranged in parallel and linked together by a distributor and a collector in perpendicular position. This basic structure designated as two-scale elementary Z-ladder has been intensively investigated in the literature. Three elementary Z-ladders are then arranged in parallel, connected by an intermediate distributor and a collector to form a 3-scale circuit. Likewise, three 3-scale circuits are arranged in parallel to form a 4-scale fluidic network, connected by a principal distributor and a principal collector. With this constructing measure, the multi-scale fluidic network has a topology [10,3,3]: “10” parallel mini-channels in an elementary Z-ladder, “3” 2-scale ladders in each 3-scale circuit and “3” 3-scale circuits to construct the entire 4-scale fluidic network.

A prototype plate embodying the multi-scale structured fluidic network was fabricated in LTEN, France by digitally-assisted carving. It is made of Aluminum, with an overall dimension of 250 mm in length (L), 250 mm in width (W) and 10 mm in thickness. The channel depth is identical (e = 1 mm) for the entire multi-scale network including 90 minichannels and all the connections. Each mini-channel has a square cross-section of 1 mm × 1 mm (hydraulic diameter D_h = 1 mm; aspect ratio AR = 1) and a channel length of 50 mm. Detailed dimensions for the connecting distributors and collectors may be found in Table 1 of [38].

Numerous gaskets were placed around the whole network to prevent the water leakage, and between neighboring channels to prevent the fluid bypass between parallel channels. Moreover, a number of bolts were used for further sealing. A photo view of the single aluminum plate is shown in Fig. 1a. A concept of novel plate-type heat exchanger having three such multi-scale structured plates stacked one above another is shown in Fig. 1b. Note that this dismountable way of assembling using gaskets is practical and effective for unit prototype. Nevertheless for massive operations, it becomes difficult to handle and expensive. Techniques such as the use of partition foils e.g., [18,19], bonding or welding [5] should be employed.

3. Methodologies

Both numerical and experimental approaches were adopted. CFD simulations were performed to characterize local temperature fields and thermal performances for the single plate heat sink and for the two-fluid plate heat exchanger. In parallel, the single plate heat sink prototype was also experimentally tested to compare with the CFD results.

3.1. Experimental set-up and measuring procedure

The experimental procedure was designed such that the base surface of the aluminum plate was heated by a uniform heat flux q_w (W m^{-2}). A coolant (water) was circulated from the principal inlet to the principal outlet of the multi-scale fluidic network at different flow-rates so as to remove the heat absorbed by the heat sink plate, as shown in Fig. 2a. The measurement of temperature at the principal inlet and outlet and at various locations of the prototype could then indicate the local temperature profiles as well as the global thermal performance of the heat sink.

Fig. 2b and c show a schematic view and a photo view of the test section. In order to seal the studied fluidic network, an aluminum cover (part A) was used and fastened with the multi-scale structured plate by

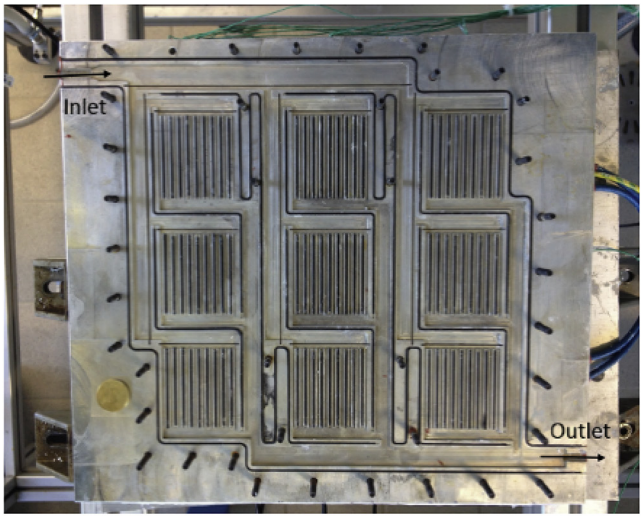

(a)

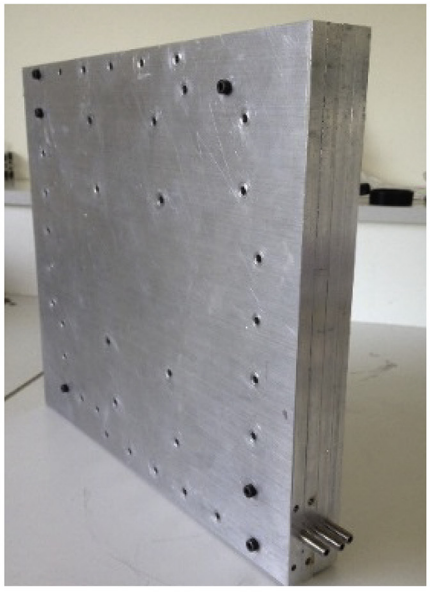

(b)

Fig. 1. Photo view of the single aluminum prototype (a) having multi-scale fluidic network embedded, and a plate-type heat exchanger (b) having 3 such plates stacked one above another.

Table 1
Physical properties of fluid and solid used for simulations (290 K < T < 373 K) [42,43].

Water	Density [kg m^{-3}]	$\rho = 999.79 + 5.29 \times 10^{-2}T - 7.63 \times 10^{-3}T^2 + 4.37 \times 10^{-5}T^3 - 1.43 \times 10^{-7}T^4$
	Specific heat [J kg^{-1} K^{-1}]	$C_p = 4.21 \times 10^3 - 2.88 \times T + 7.29 \times 10^{-2}T^2 - 7.40 \times 10^{-4}T^3 + 2.98 \times 10^{-6}T^4$
	Viscosity [Pa s]	$\nu = 1.79 \times 10^{-3} - 5.49 \times 10^{-5}T + 9.55 \times 10^{-7}T^2 - 8.61 \times 10^{-9}T^3 + 3.05 \times 10^{-11}T^4$
	Thermal conductivity [W m^{-1} K^{-1}]	$\lambda = 5.63 \times 10^{-1} + 1.96 \times 10^{-3}T - 8.27T^2$
Aluminum	Density [kg m^{-3}]	$\rho = 2700$
	Specific heat [J kg^{-1} K^{-1}]	$C_p = 5.09 \times 10^2 + 1.84T - 1.81 \times 10^{-3}T^2$
	Thermal conductivity [W m^{-1} K^{-1}]	$\lambda = 2.06 \times 10^2 + 1.66 \times 10^{-1}T - 2.00 \times 10^{-4}T^2$

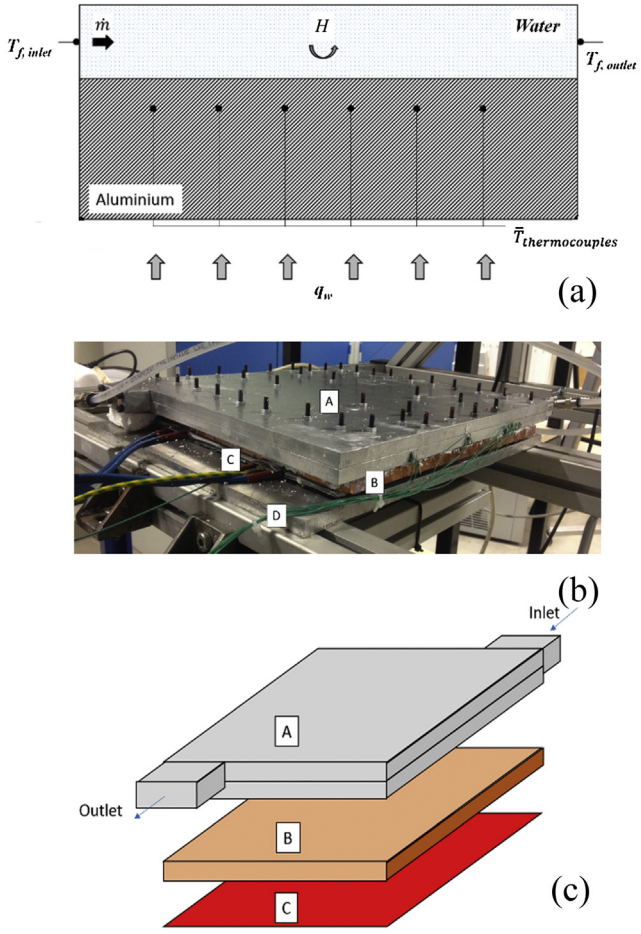

Fig. 2. Thermal performance testing of the multi-scale structured heat sink. (a) schematic view of the testing principle; (b) photo view of the test-section without insulation; (c) schematic view of the test-section.

nuts and bolts. The tightness of the test section was verified before every test. A heat generating resistor (part C) (mica Jeannot, 1200 W max, 36 V) connected to a Kepco power supply (KLP 36-60) was used to create heat power input, controlled by a LabVIEW program developed in house via a GPIB port. A copper plate of 10 mm thickness (part B) was inserted between the Aluminum heat sink plate and the heat generating resistor so as to attenuate the spreading thermal resistance and homogenize the heat flux at the base surface. The combined test-section was then insulated except for the bottom side where the heat generating resistor was located. The reason is that the power supply of the resistor will be cut off to protect the resistor when the temperature difference between two sides of the resistor plate grows to a certain value. To avoid this cut-off of heat supply, a ventilation unit has been installed below the resistor to guarantee its temperature below 120 °C, providing steady-state conditions for the experiments.

The mass flow-rate (m) of cooling water was controlled and adjusted by a precise pump-mass controller (VWR, REGLO-Z, 32–3200 mL min^{-1}). A flowmeter (Kobold DPL, ± 2.5% precision) was located between the mass controller and the test section so as to measure the inlet water flow-rate. Two thermocouples of type K (± 0.2 K precision) were installed in the fluid circuit near the global inlet and outlet of the network so as to measure the inlet ($T_{f,\,inlet}$) and outlet ($T_{f,\,outlet}$) temperature of the cooling water. Other 13 thermocouples of type K were instrumented in the multi-scale structured plate to measure the local temperature at various locations, as may be observed in Fig. 3. The centers of all 13 thermocouple beans were aligned in the same plane at 1 mm below the bottom surface of the fluid network, as shown in Fig. 2a. All the thermocouples (part D) were connected to an Agilent 34902a card (± 0.1% precision) for data recording. Experiments were conducted at steady state condition. All experimental data were captured when all physical parameters were stable (about 20 min for each measurement).

Experiments were carried out for both the basic network (without baffles) and the optimized network (equipped with optimized baffles). The perforated baffles are basically in the form of thin rectangular shape slices made of PMMA (1 mm in thickness). More details on the optimization of orifice sizes and their insertions may be found in our previous hydrodynamic study [38]. An uncertainty analysis was performed following the method of Moffat [41]. The estimated measurement uncertainty is within ± 3.1% for the mean Re_{ch}, ± 1.5% for the transferred heat flux q_w (Eq. (1)) and ± 1.5% for the global heat transfer coefficient H (Eq. (2)), respectively.

3.2. CFD simulation parameters

In this study, geometries and meshes were generated using different modules of ANSYS Workbench 16.1. Pure water was chosen as working fluid while the solid part was Aluminum. The operational pressure was fixed at 101325 Pa. The physical properties of fluid and solid were considered as temperature dependent, using the polynomial fitting correlations listed in Table 1. It should be noted that the expansion properties of solid material were ignored in our study.

For the fluid zone, constant mass flow-rate of water at about 293 K (small variation corresponding to the real tested condition) was given at the global inlet as the inlet boundary condition. Seven inlet mass flow-rates (m) were tested: 6.8×10^{-3} kg s^{-1}; 9.9×10^{-3} kg s^{-1}; 1.87×10^{-2} kg s^{-1}; 2.77×10^{-2} kg s^{-1}; 3.66×10^{-2} kg s^{-1}; 4.52×10^{-2} kg s^{-1}; 5.54×10^{-2} kg s^{-1}, corresponding to the mean channel Reynolds number (mean Re_{ch}) of 75; 110; 208; 307; 406; 502; 605, respectively. The boundary condition of the outlet was set as pressure-outlet with zero static pressure. Non-slip wall condition was applied. For the solid zone, a uniform heat flux (q_w) was set at the base surface of the heat sink. The q_w value for each testing case was set as the real heat power density calculated based on the experimentally measured heat exchange rate removed by the cooling water at steady-state.

$$q_w = \frac{mC_p(T_{f,outlet} - T_{f,inlet})}{L \times W} \quad [\mathrm{W{\cdot}m^{-2}}] \tag{1}$$

where L (m) and W (m) are the length and width of the base surface. Other walls of the solid zone were considered as adiabatic.

Fluid flow simulations were performed under steady-state with heat transfer, using ANSYS Fluent code (version 16.1). The viscous heating

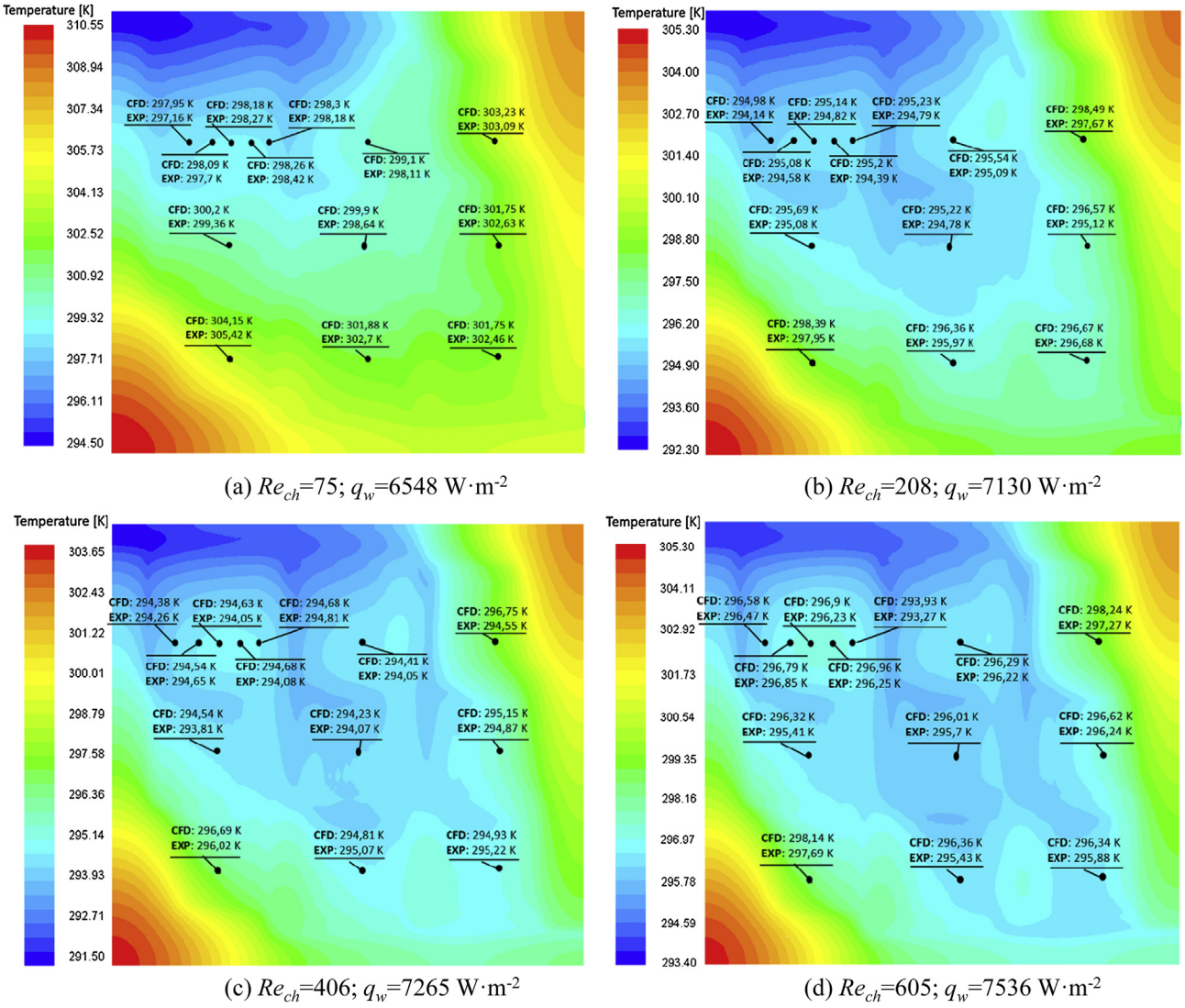

Fig. 3. Temperature profiles of the thermocouple cutting plane. (a) mean Re_{ch} = 75; (b) mean Re_{ch} = 208; (c) mean Re_{ch} = 406; (d) mean Re_{ch} = 605.

effect and gravity effect were also considered. Laminar flow model was used under very low velocity conditions (mean Re_{ch} < 100). Turbulent k-ε RNG model was adopted for higher mean Re_{ch} (200–600) mainly because of the possible presence of detached flows, local vortex and micro-turbulences even still at theoretical laminar flow regime. The fluid-structure interactions and the influences of inertial force on the flow profiles have been addressed in detail in our previous work [38]. Standard SIMPLE method was used for the pressure-velocity coupling. For discretization, standard method was chosen for pressure and first-order upwind differentiation for momentum. The solution was considered to be converged when (i) the fluid inlet static pressure and outlet temperature were constant from one iteration to the next (less than 0.5% variation) and (ii) the normalized residuals of all monitoring parameters were lower than the order of magnitude of 10^{-5}. Note that only the basic network without baffles was simulated. The simulation of the optimized network after insertion of various baffles for more uniform flow distribution as suggested in [38] didn't succeed due to numerical instabilities.

A grid independence study was performed using three meshes with different densities: medium mesh (5 segments per millimeter; 0.45 million elements in total); fine mesh (10 segments per millimeter; 1.94 million elements in total) and very fine mesh (15 segments per millimeter; 5.14 million elements in total). Simulation results with an inlet mass flow-rate of 5.54×10^{-2} kg s^{-1} (mean Re_{ch} = 600) indicated a difference of 4.7% on the inlet pressure between the medium mesh and the fine mesh, and of 1.5% between the fin and very fine mesh. Comparisons were also made on the fluid outlet temperature and the solid maximum temperature. For fluid outlet temperature, the difference is 0.8% between medium mesh and fine mesh, and 0.3% between the fine and very fine mesh. For solid maximum temperature, the difference is 1.0% and 0.4%, respectively. Hence, the fine mesh was selected as a compromise between the calculation time and the precision. It had 1.94 million elements in total, with 0.78 million structured hexahedral elements for the fluid zone and 1.16 million unstructured elements for the solid zone. Relatively higher mesh density was applied for the fluid zone.

4. Results and discussion

In this section, results obtained on the thermal performances for the multi-scale structured fluidic network are presented. For the single plate heat sink case, both CFD and experimental results are presented and compared. For the two-stream plate-type heat exchanger case, only the numerical results are obtained and shown.

4.1. Thermal performance of a heat sink containing the multi-scale fluidic network

Once the CFD simulations were performed, a cutting plane was created at the same position where the center of thermocouples' beans were experimentally implanted. Fig. 3 shows the simulated temperature fields on this cutting plane, under four different mean Re_{ch} conditions (75; 208; 406; 615). The temperature values of 13 measuring points obtained numerically (CFD) and experimentally (EXP) are also indicated in Fig. 3 for comparison. Good agreement between CFD and experimental results may be observed at different positions of the heat sink plate, with the maximum difference smaller than 0.78 K regarding the max-min temperature difference of the cutting surface being about 15 K.

Fig. 3 clearly demonstrates the cooling effect of the multi-scale fluidic network, especially at mean Re_{ch} larger than 200. In fact, a number of cooled zones appear, visibly located at various elementary Z-ladders and at distributors/collectors of different scales. The lowest temperature zone appears at the global entrance (principal distributor) because of the cold inlet temperature of cooling fluid (~290 K). The hotspots are located at the down-left and top-right corners of the plate, mainly due to the absence of the cooling fluidic network at these zones. The global temperature profile on the thermocouple cutting surface shows some kind of symmetry character regarding the inlet/outlet diagonal line. Locally, the cooling effect is a bit more effective at the top-right part than the down-left part, mainly because of the slightly geometrical asymmetry as well as the inertial effect of cooling fluid flow (cooling fluid flowing from left to right in the principal distributor).

It may also be observed in Fig. 3 that the allocation of thermocouple measuring points don't well cover the whole cutting surface. Actually, no thermocouple has been instrumented at the periphery of the cutting surface where the hotspots (down-left and top-right corners) and the cold zone (top-left corner) are located. As a result, the temperature profile based on the thermocouple measurements is not representative for calculating some thermal performance indicators, which will be further discussed later.

More details on the temperature profiles for both the fluid and solid parts of the multi-scale structured heat sink plate are given in Fig. 4. For the solid part, similar pattern may be observed for different mean Re_{ch} tested. Two hotspots are located at the bottom-left corner and the top-right corner mainly due to the conception default since no fluidic paths are embedded in these zones. Temperature rises because the heat

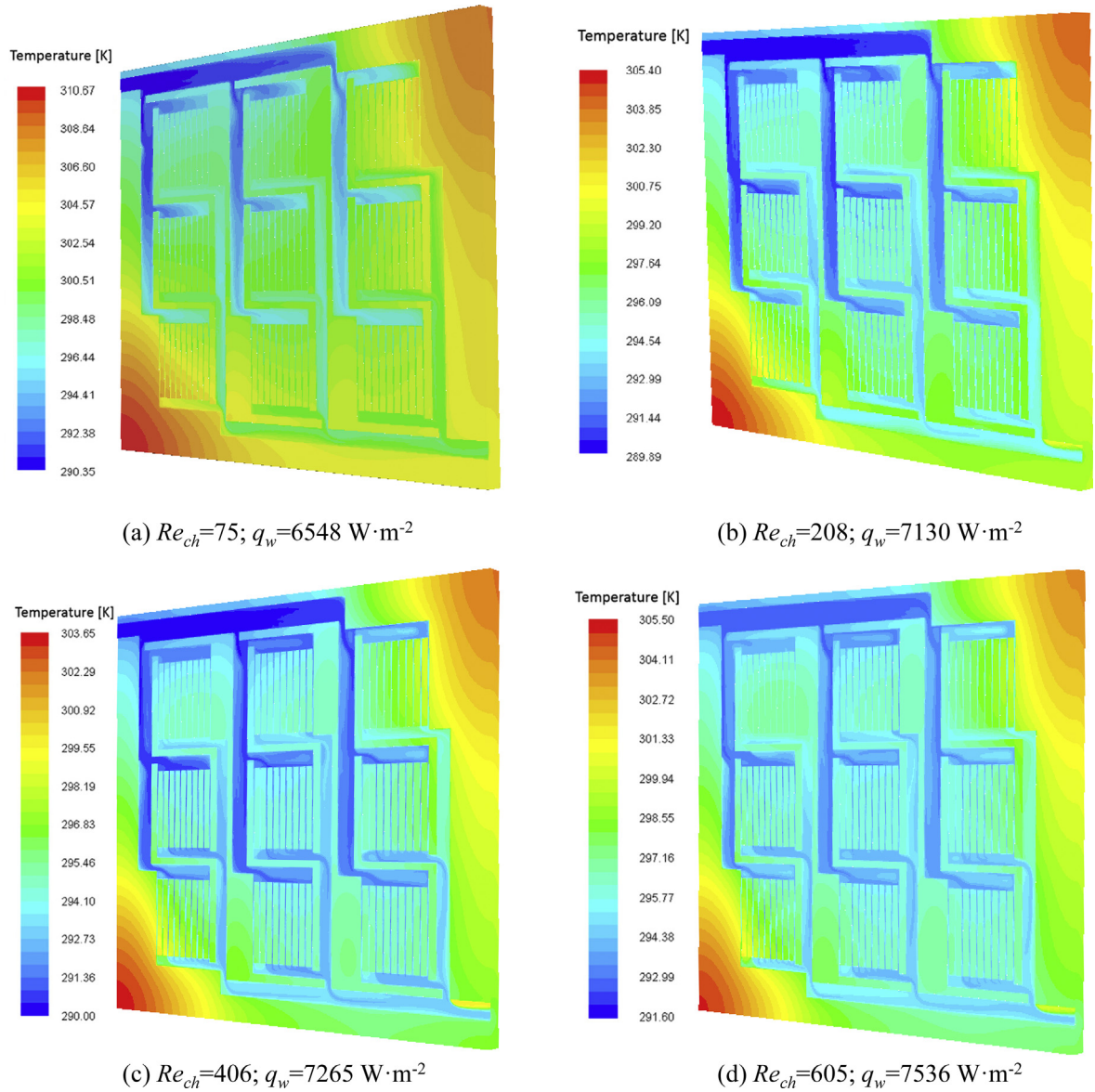

Fig. 4. Temperature profiles of the fluid and solid parts. (a) mean Re_{ch} = 75; (b) mean Re_{ch} = 208; (c) mean Re_{ch} = 406; (d) mean Re_{ch} = 605.

removal by convection is lacking.

Concerning the fluid part, some different thermal behaviors may be observed. At mean $Re_{ch} = 75$, low-temperature fluids are located in the principal distributor as well as in the intermediate distributors, close to the global inlet of the fluidic network. The longer residence time they stay in the network, the higher amount of heat flux will be absorbed by the fluids, getting higher temperature (except for corner elementary ladders which are greatly influenced by the hotspots). After passing through the mini-parallel channels, fluids in the collector parts of different scales are generally heated up because of the relatively longer residence time.

At higher mean Re_{ch} (Fig. 4c and d), cold zones grow towards the global outlet of the fluidic network, demonstrating the effects of the cooling network. Locally low-temperature fluids may be observed at different collectors, because of the relatively higher fluid velocity thus shorter residence time to absorb the heat power. A clear hotspot for the fluid zone may be observed at very close to the global outlet of the network, which is the stagnant area having very low fluid velocity. In brief, the local fluid temperature is greatly influenced by its local velocity profile.

The temperature profiles of the fluid and solid parts help in knowing the regions that are influenced by flow distribution non-uniformity. For each elementary Z-ladder, the flow distribution non-uniformity may not have a significant influences on the temperature field because of the short distances between neighboring mini-channels (3 mm wall thickness). However, the flow distribution non-uniformity among the 9 elementary ladder could have an impact on the thermal performance of the multi-scale fluidic network. In fact, it may be observed from Fig. 4 that the temperature of the lower-left part is higher than that of the upper right part. This is because the ladders of the left column close to the global inlet are generally underfed, leading to lower heat removal capability. The fluid flow tends to skip the nearest ladders they pass by because of the inertial forces, as has been discussed in detail in our earlier work [38]. In future designs measures may be considered for preferentially equalizing the flow distribution among different elementary ladders.

Having discussed the local temperature profiles as well as their relation to the local velocity profiles, now we are interested in knowing the values of some indicators showing the global thermal performances of the single plate multi-scale structured heat sink, including the transferred heat flux (q_w), the global heat transfer coefficient (H) and the heat sink thermal resistance (R_{th}).

Fig. 5 shows the values of heat flux q_w ($\mathrm{W\,m^{-2}}$) absorbed by the cooling fluid, calculated based on Eq. (1). Recall that only the experimentally measured data are presented in Fig. 5 and these values have been used as inputs for the boundary condition of the base surface in CFD simulations. It can be seen that the q_w value ranges between about 6.5 and 7.5 $\mathrm{kW\,m^{-2}}$, corresponding to the exchanged heat power removed by the cooling fluid of about 400 to 470 W. The heat losses have then accounted for about half of the total heat input provided by the heat generating resistor (900 W). The high amount of heat losses is mainly due to the implementation of a ventilation unit to guarantee the resistor temperature below 120 °C, as explained above. Note that the q_w values for the basic network and for the optimized network are very close, also because of the heat losses.

Now we are interested in the global heat transfer coefficients (H) of the heat sink which is generally defined as the ratio between the heat transfer rate (W) and the product of heat transfer surface area ($\mathrm{m^2}$) and the temperature difference between the solid and the fluid (K). Nevertheless, a number of H values could be calculated depending on which value of transfer surface area and which value of temperature difference are used for the calculation. Here we introduce the global heat transfer coefficient (H) as defined in Eq. (2):

$$H = \frac{q_w}{\bar{T}_{cuttingplane} - \bar{T}_{fluidinlet-outlet}} \quad [\mathrm{W{\cdot}m^{-2}{\cdot}K^{-1}}] \tag{2}$$

where q_w is the transferred heat flux (Eq. (1)), the corresponding heat transfer surface area is then the heating surface of the heat sink ($W \times L$). $\bar{T}_{cuttingplane}$ is the mean temperature of the thermocouple cutting plane in the solid part. Note that experimentally it is the algebraic average of the 13 measurements of the instrumented thermocouples while numerically it is the surface-area averaged temperature of the cutting surface. $\bar{T}_{fluidinlet-outlet}$ is the mean fluid temperature between the global inlet and outlet.

Fig. 6 presents the H values of the multi-scale structured heat sink at various mean Re_{ch} numbers. Generally, both CFD and experimental H values augment with increasing mean Re_{ch}. It can be noticed that at the same mean Re_{ch}, the H values experimentally measured are remarkably higher than those calculated numerically. This disagreement is mainly due to the different ways for calculating $\bar{T}_{cuttingplane}$. In experiments, it is simply the algebraic average of only 13 measurements of thermocouples. Hence, it cannot correctly reflect the real mean temperature of the cutting surface. In fact, the hotspots and the cold zones located at the periphery of the cutting surface as shown in Fig. 3 are not taken into account. The value of $\bar{T}_{cuttingplane}$ calculated by this way is lower than the surface-sera average temperature of the cutting surface obtained numerically, resulting in the overestimated values of experimental global heat transfer coefficient H as shown in Fig. 6. On the contrary, the CFD H values are more credible and representative, increasing from about 1100 to 3000 $\mathrm{W\,m^{-2}\,K^{-1}}$ when mean Re_{ch} increases from 75 to 600.

Another feature that may be observed from Fig. 6 is that the H values for the optimized network equipped with perforated baffles are about 20–28% higher than those for the basic network. The reason for very close q_w values but different H values is that the mean temperature $\bar{T}_{cuttingplane}$ of the 13 sampling points (where thermocouples are installed) for the optimized network is lower than that for the basic network. Higher values of H could then be obtained when heat flux is almost equal. However, caution must be taken when interpreting these results because they are calculated based on the measurements of thermocouples with limited sampling number and arbitrary repartition. For future studies, a higher quantity and a better repartition of thermocouple measuring points should be implemented to obtain more representative and exploitable temperature profiles.

Finally, the global thermal resistance (R_{th}) of the multi-scale structured heat sink is calculated based on the CFD results obtained, defined as:

$$R_{th} = \frac{T_{w,max} - T_{fluid,inlet}}{q_w WL} \quad [\mathrm{K{\cdot}W^{-1}}] \tag{3}$$

where $T_{w,max}$ is the maximum temperature of the heat sink base plate and $T_{fluid,inlet}$ is the inlet temperature of cooling water.

Using this definition, the R_{th} values of the multi-scale structured heat sink as a function of pressure drop are computed and shown in

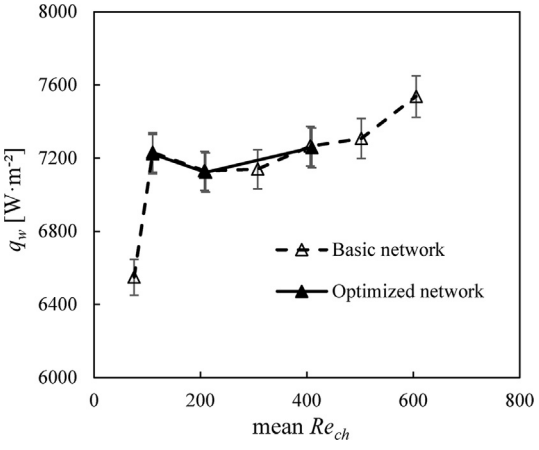

Fig. 5. Heat flux q_w absorbed by the cooling fluid as a function of mean Re_{ch}.

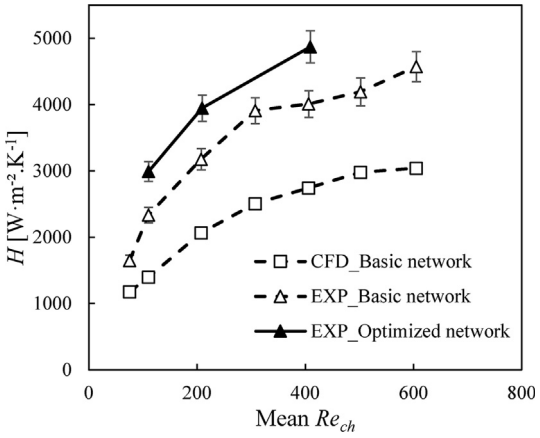

Fig. 6. Global heat transfer coefficient H of the multi-scale structured heat sink as a function of mean Re_{ch}.

Fig. 7. The available R_{th} data for other micro- or mini-channel heat sinks [15,44,45] in the literature are also drawn on Fig. 7 for comparison. It may be found that the global thermal resistance decreases with the increasing pressure drop. This is logical because pressure drop is proportional to the total flow-rate (also the mean Re_{ch}) of cooling fluid (Fig. 6 of [38]). Lower $T_{w,max}$ could be achieved at higher total flow-rate of cooling fluid, implying smaller values of R_{th}.

It can also be observed that at the same pressure drop, the R_{th} values for the multi-scale structured heat sink are remarkably smaller than those of micro- or mini-channels heat sinks tested in the literature. This is mainly because of the larger channel sizes as well as the larger overall dimension of our heat sink, showing again the advantages of milli-structured devices compared to micro-structured equipment. Another highlighted attractive feature of our heat sink is the multi-scale structure and parallel arrangement of elementary Z-ladders. Even with multiple intermediate connections (distributors & collectors), lower global thermal resistance can still be achieved under the same pressure drop condition.

It should also be noted that the heat sinks compared in Fig. 7 are proposed for the cooling of electronic devices (e.g., CPU). As a result, they usually have a very small overall dimension and small channel sizes (*micro-structured micro heat sinks*), but with a much higher transferred heat flux q_w by one or two orders of magnitude than our tested conditions. For a more fair comparison with the literature data, miniaturization by resizing the multi-scale structured heat sink must be done in order to better fit the requirements of electronic cooling. A benchmark testing (same overall size, heat flux, inlet temperature, etc.) condition for different designs is also need for more convincing evaluation and comparison of hydrothermal performances.

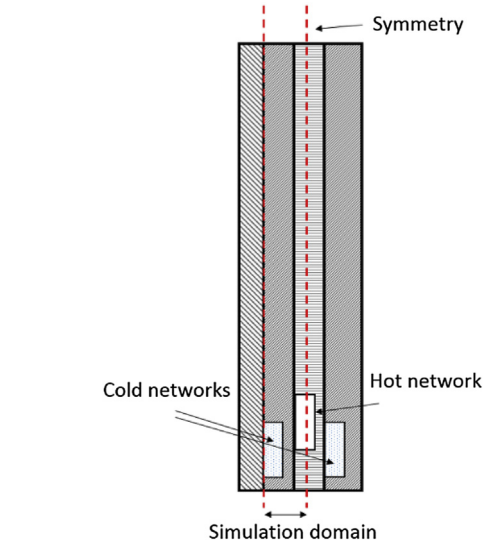

Fig. 8. Simulation schema for the two-fluid plate-type heat exchanger prototype.

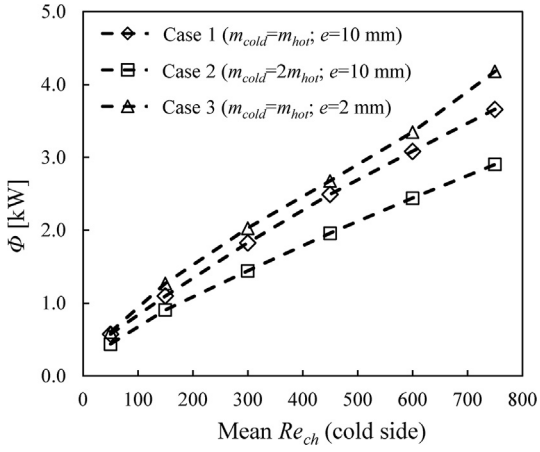

Fig. 9. Heat transfer rate Φ as a function of mean Re_{ch} for three tested cases.

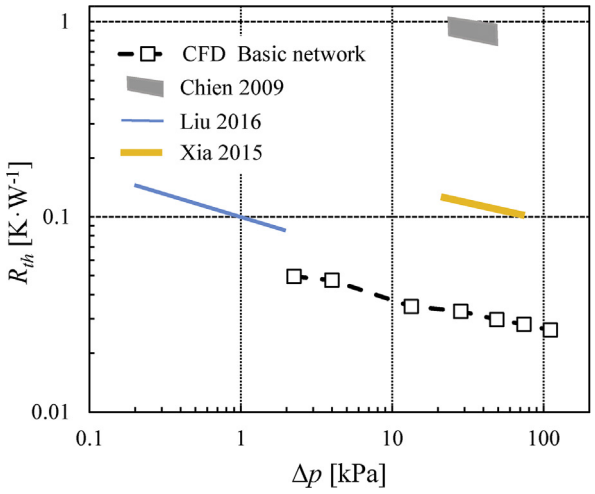

Reference	Base surface W×L (cm²)	Channel characteristics	q_w (W·cm⁻²)
[Chien 2009]	0.62×1.8	11 microchannels; 200 μm × 400 μm × 10 mm	100
[Xia 2015]	1×1	30 microchannels; 100 μm × 300 μm × 4 mm	200
[Liu 2016]	4.1×6.4	13 mini-channels; 2.65 mm × 1 mm × 40 mm	8
Current study	25×25	90 mini-channels; 1 mm × 1 mm × 50 mm	~0.7

Fig. 7. Overall thermal resistance R_{th} (K W^{-1}) as a function of pressure drop for various micro or milli-channels heat sinks.

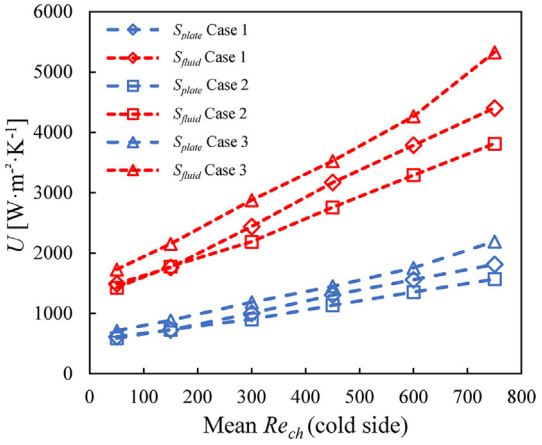

Fig. 10. Overall heat transfer coefficient U as a function of mean Re_{ch} for three tested cases.

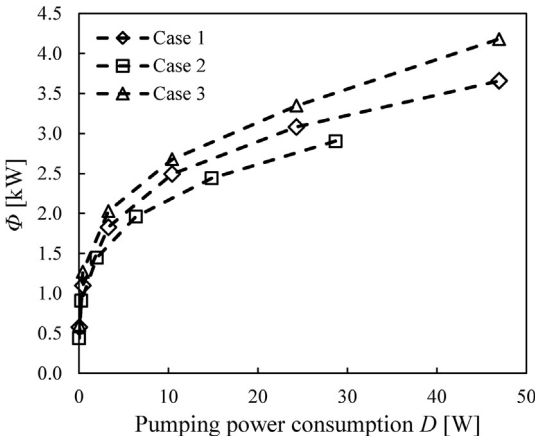

Fig. 11. Heat transfer rate Φ as a function of the pumping power consumption D for three tested cases.

4.2. Thermal performances of the two-fluid plate heat exchanger

Finally, we are interested in knowing the global thermal performance of the novel plate-type heat exchanger with multi-scale structured plate surfaces. The prototype of such heat exchanger having 4 plates (2 multi-scale structured plates for cold fluid; 1 plate for hot fluid and one cover plate without fluidic network) has already been illustrated in Fig. 1b. Experimental results are not available at this stage due to assembling difficulties, the results presented here were obtained through CFD simulations.

Only one and a half plates were simulated by taking into account the symmetry character of the sandwiched-type geometry, as shown Fig. 8. More precisely, the simulated geometry consists in a solid part of 250 mm in width, 250 mm in length and 10.5 mm (or 2.5 mm) in thickness. On one of its faces, a cold four-scale fluidic network is etched with 1 mm in depth. On the opposite face, a hot four-scale network is etched with 0.5 mm in depth.

The working fluids were set as hot and cold water. Their inlet temperature was 293 K and 338 K, respectively (ΔT_{max} = 45 °C). Physical properties of water and aluminum were set as temperature dependent, as shown in Table 1. Three cases of working condition were tested, with the mean Re_{ch} (cold side) varying from 50 to 750:

- Case 1: $m_{cold} = m_{hot}$; plate thickness e = 10 mm
- Case 2: $m_{cold} = 2m_{hot}$; plate thickness e = 10 mm
- Case 3: $m_{cold} = m_{hot}$; plate thickness e = 2 mm

Fig. 9 shows the heat transfer rate (Φ) of the multi-scale structured plate-type heat exchanger for three tested cases, calculated by Eq. (4).

$$\Phi = m_{hot}\bar{C_{p_{hot}}}(T_{hot,in} - T_{hot,out}) = m_{cold}\bar{C_{p_{cold}}}(T_{cold,out} - T_{cold,in})[\mathrm{W}] \quad (4)$$

where $\bar{C_p}$ is the average heat capacity of fluid at the mean temperature between inlet and outlet.

It may be observed that the Φ value for each case increases almost linearly with the increasing mean Re_{ch}. This is mainly because of the enhanced convection heat transfer at higher velocities (Re_{ch}). By comparing the Φ values for Case 1 and Case 2, one may observe that balanced flow (case 1) produces higher heat transfer rate than unbalanced flow (case 2). This may be explained by the fact that mean Re_{ch} is calculated based on the cold side. At certain mean Re_{ch}, m_{cold} is the same but m_{hot} is reduced by a factor of 2 for Case 2, resulting in decreased convection coefficients of the hot side and thus the reduced heat transfer rate. By comparing Case 1 and Case 3, it may be observed that thinner plate thickness augments the heat transfer rate. When mean Re_{ch} increases from 50 to 750, the Φ value for Case 3 (e = 2 mm) increases from 0.61 kW to 4.18 kW, 5.2% to 14.2% higher than those for Case 1 (e = 10 mm). The reduced conduction thermal resistance of the thinner plate enhances the heat transfer from the hot flow to the cold flow, which is in line with the finding of Yang et al. [18]. In brief, higher channel velocity and thinner plate thickness enhance the convection and conduction heat transfer, respectively. Note that the volumetric power of this multi-scale structure plate heat exchanger could reach about 25.6 MW m^{-3} under our tested conditions.

Fig. 10 shows the overall heat transfer coefficient (U) of the multi-scale structured plate-type heat exchanger for three tested cases, calculated following the LMTD method (counter-current configuration).

$$U = \frac{\Phi}{S\Delta T_{LMTD}} \quad [\mathrm{W{\cdot}m^{-2}{\cdot}K^{-1}}] \quad (5)$$

$$\Delta T_{LMTD} = \frac{(T_{hot,in} - T_{cold,out}) - (T_{hot,out} - T_{cold,in})}{ln\frac{T_{hot,in} - T_{cold,out}}{T_{hot,out} - T_{cold,in}}} \quad [\mathrm{W{\cdot}m^{-2}{\cdot}K^{-1}}] \quad (6)$$

Depending on the choice of heat transfer surface, two sets of values for U can be calculated, as both shown in Fig. 10: the blue ones based on the plate surface area (S_{plate} = 0.0625 m^2) whereas the red ones based on the bottom area of the fluidic network (S_{fluid} = 0.0257 m^2). It may be observed that for each set of U values, Case 3 (balanced flow, thinner plate) always has the best results among the three cases tested. The U values for Case 3 range from 710 to 2200 W m^{-2} K^{-1} (or from 1700 to 5300 W m^{-2} K^{-1}) when mean Re_{ch} (cold side) increases from 50 to 750.

The heat transfer rate Φ (W) as a function of the pumping power consumption D (W) of the heat exchanger is shown in Fig. 11, the latter is calculated based on the Eq. (7):

$$D = \frac{m_{hot}}{\bar{\rho_{hot}}} \times \Delta p_{hot} + \frac{m_{cold}}{\bar{\rho_{cold}}} \times \Delta p_{cold} \quad [\mathrm{W}] \quad (7)$$

It can be observed that the higher heat transfer rates may be achieved by consuming more pumping power. For a given duty of heat transfer rate, Case 3 consumes the least pumping power. In other words, at the same pumping power consumption, Case 3 could achieve the highest heat transfer rate. The positive effect of heat transfer intensification measures (higher velocity, thinner plate) is again highlighted.

One may also observe that the pumping power consumption of this novel plate-type heat exchanger is relatively low (< 50 W) under the tested conditions (mostly laminar). Higher heat transfer rates can still be expected by augmenting the flow-rate of the two fluids.

5. Conclusion and perspectives

In this paper, the thermal performances of a multi-scale structured fluidic network has been investigated. We will now summarize the main

findings, further discuss some interesting issues and provide some new ideas for the future research.

Main findings are listed as follows.

- *For the mini-channel heat sink:* the heat removal tests show a global heat transfer coefficient (H) of about 1000 to 3000 $W\,m^{-2}\,K^{-1}$ when mean Re_{ch} ranges between 75 and 600. At the same pressure drop, the overall thermal resistances (R_{th}) of the novel concept are remarkably smaller than some micro- or mini-channels heat sinks reported in the literature. The attractive features of the multi-scale structure and parallel arrangement of Z-ladders are highlighted.
- *For the two-fluid plate-type heat exchanger:* the overall heat transfer coefficients (U) based on the surface area of base plate range from 710 to 2200 $W\,m^{-2}\,K^{-1}$ when mean Re_{ch} (cold side) increases from 50 to 750. The effects of higher channel velocity and thinner plate thickness on the enhancement of heat transfer are clearly shown.

The investigations performed also have some limitations. Some of them are in connection to the multi-scale concept while others are due to the approaches used.

- The diagonal configuration for the elementary Z-ladder as well as for the multi-scale network will lead to the hotspots at the two corners without cooling channels embedded. This is a conception default and some additional circuits may have to be implemented in those zones. Moreover, some other multi-scale concepts with a combination of Z, U, or I configurations will also be interesting, but implying more complicated geometries.
- Relatively uniform flow distribution is shown to be achievable even for 90 parallel mini-channels by installing a number of optimized baffles [38]. Nevertheless, the augmentation on the thermal performance by more uniform flow distribution is still veiled. This is mainly due to the heat losses during the experiments and the difficulty in simulating the optimized network. Additional work should be done on this point, e.g., using flow equivalent resistance model to represent the baffle characteristics.

Our future work will focus on the following aspects. Firstly, it will be interesting to design a multi-scale structured (micro-) heat sink of small overall dimension (typically $2 \times 2\,cm^2$), for the purpose of electronic cooling with a high heat flux (e.g., 10^2–$10^3\,W\,cm^{-2}$). A benchmark testing condition (same overall size, heat flux, inlet temperature, etc.) should be useful to demonstrate the benefits of multi-scale structuration concept compared to simple parallel-flow arrangements. The influences of flow distribution uniformity on the thermal performances could be much more significant at very high heat flux, as reported in the recent literature [46,47]. Moreover, a pertinent criterion that accounts for both the heat transfer and dissipations will be interesting to be introduced and compared. Another possible way is the Pareto-front optimization under two-objectives of thermal resistance and pressure drop, as has been reported in [22].

Secondly, a benchmark testing of the plate heat exchanger and some commercially available products will provide a good comparison on the hydrothermal performances under the same working conditions. Thin plates (typically 2–3 mm) with the multi-scale fluidic network embedded should be fabricated, either by digitally-assisted drilling or by advanced additive manufacturing techniques, then assembled and tested. The comparison on the volumetric power ($MW\,m^{-3}$) at the same pumping power consumption (W) will showcase the advantages of the *multi-scale structuration concept*.

Finally, the application of the multi-scale structured plate heat exchangers as latent heat thermal energy storage system with phase change materials (PCM) or composite materials incorporated is our ongoing work. Compared to conventional shell-and-tube type or double pipe configurations [48–50], better thermal performances are expected owing to the benefits of multi-scale structuration.

6. Declarations of interest

None.

Acknowledgements

This work was supported by the “Région Pays de la Loire” (Nouvelle équipe de recherche project); and the European Commission H2020 MSCA programme (for the EU H2020-MSCA-RISE-2016-734340-DEW-COOL-4-CDC project, EU Commission). Authors are grateful to Mr. Gwenaël BIOTTEAU for the fabrication of the prototypes.

References

[1] T. Van Gerven, A. Stankiewicz, Structure, energy, synergy, time-the fundamentals of process intensification, Ind. Eng. Chem. Res. 48 (5) (2009) 2465–2474, https://doi.org/10.1021/ie801501y.
[2] S. Becht, R. Franke, A. Gießelmann, H. Hahn, Micro process technology as a means of process intensification, Chem. Eng. Technol. 30 (2007) 295–299, https://doi.org/10.1002/ceat.200600386.
[3] J.J. Brandner, L. Bohn, T. Henning, U. Schygulla, K. Schubert, Microstructure heat exchanger applications in laboratory and industry, Heat Transf. Eng. 28 (8–9) (2007) 761–771, https://doi.org/10.1080/01457630701328528.
[4] Y. Fan, L. Luo, Recent applications of advances in microchannel heat exchangers and multi-scale design optimization, Heat Transf. Eng. 29 (5) (2008) 461–474, https://doi.org/10.1080/01457630701850968.
[5] T. Dixit, I. Ghosh, Review of micro- and mini-channel heat sinks and heat exchangers for single phase fluids, Renew. Sustain. Energy Rev. 41 (2015) 1298–1311, https://doi.org/10.1016/j.rser.2014.09.024.
[6] J.-F.O. Portha, L. Falk, J.-M. Commenge, Local and global process intensification, Chem. Eng. Process. Process Intensif. 84 (2014) 1–13, https://doi.org/10.1016/j.cep.2014.05.002.
[7] J.J. Brandner, Microstructure devices for process intensification: influence of manufacturing tolerances and design, Appl. Therm. Eng. 59 (1–2) (2013) 745–752, https://doi.org/10.1016/j.applthermaleng.2013.01.003.
[8] V. Hessel, H. Löwe, A. Müller, G. Kolb, Chemical Micro Process Engineering: Processing and Plants, Wiley-VCH Verlag GmbH & Co., 2005.
[9] A. Bejan, S. Lorente, Constructal tree-shaped flow structures, Appl. Therm. Eng. 27 (4) (2007) 755–761, https://doi.org/10.1016/j.applthermaleng.2006.10.008.
[10] J. Lee, S. Kim, S. Lorente, A. Bejan, Vascularization with trees matched canopy to canopy: diagonal channels with multiple sizes, Int. J. Heat Mass Transf. 51 (7–8) (2008) 2029–2040, https://doi.org/10.1016/j.ijheatmasstransfer.2007.06.015.
[11] C. Renault, S. Colin, S. Orieux, P. Cognet, T. Tzédakis, Optimal design of multi-channel microreactor for uniform residence time distribution, Microsystem Technol. 18 (2012) 209–223, https://doi.org/10.1007/s00542-011-1334-7.
[12] C. Pistoresi, Y. Fan, L. Luo, Numerical study on the improvement of flow distribution uniformity among parallel mini-channels, Chem. Eng. Process. Process Intensif. 95 (2015) 63–71, https://doi.org/10.1016/j.cep.2015.05.014.
[13] M. Saber, J.M. Commenge, L. Falk, Rapid design of channel multi-scale networks with minimum flow maldistribution, Chem. Eng. Process. Process Intensif. 48 (3) (2009) 723–733, https://doi.org/10.1016/j.cep.2008.09.001.
[14] M.C. Lu, C.C. Wang, Effect of the inlet location on the performance of parallel-channel cold-plate, IEEE Trans. Compon. Packag. Technol. 29 (1) (2006) 30–38, https://doi.org/10.1109/TCAPT.2005.850539.
[15] R. Chein, J. Chen, Numerical study of the inlet/outlet arrangement effect on microchannel heat sink performance, Int. J. Therm. Sci. 48 (8) (2009) 1627–1638, https://doi.org/10.1016/j.ijthermalsci.2008.12.019.
[16] M. Saber, J.M. Commenge, L. Falk, Heat-transfer characteristics in multi-scale flow networks with parallel channels, Chem. Eng. Process. Process Intensif. 49 (7) (2010) 732–739, https://doi.org/10.1016/j.cep.2009.10.017.
[17] E.S. Cho, J.W. Choi, J.S. Yoon, M.S. Kim, Experimental study on microchannel heat sinks considering mass flow distribution with non-uniform heat flux conditions, Int. J. Heat Mass Transf. 53 (9–10) (2010) 2159–2168, https://doi.org/10.1016/j.ijheatmasstransfer.2009.12.026.
[18] Y. Yang, I. Gerken, J.J. Brandner, G.L. Morini, Design and experimental investigation of a gas-to-gas counter-flow micro heat exchanger, Exp. Heat Transf. 27 (4) (2014) 340–359, https://doi.org/10.1080/08916152.2013.849179.
[19] I. Gerken, J.J. Brandner, R. Dittmeyer, Heat transfer enhancement with gas-to-gas micro heat exchangers, Appl. Therm. Eng. 93 (2016) 1410–1416, https://doi.org/10.1016/j.applthermaleng.2015.08.098.
[20] S.A. Solovitz M. Lewis Tailored parallel micro-channel cooling for hot spot mitigation Fourteenth Intersociety Conference on Thermal and Thermomechanical Phenomena in Electronic Systems (ITherm) 2014 Orlando, FL 641 648 10.1109/ITHERM.2014.6892342.
[21] Y.T. Mu, L. Chen, Y.L. He, W.Q. Tao, Numerical study on temperature uniformity in a novel mini-channel heat sink with different flow field configurations, Int. J. Heat Mass Transf. 85 (2015) 147–157, https://doi.org/10.1016/j.ijheatmasstransfer.2015.01.093.
[22] H. Shen, X. Jin, F. Zhang, G. Xie, B. Sunden, H. Yan, Computational optimization of counter-flow double-layered microchannel heat sinks subjected to thermal resistance and pumping power, Appl. Therm. Eng. 121 (2017) 180–189, https://doi.

org/10.1016/j.applthermaleng.2017.04.058.
[23] H. Shen, Y. Zhang, C.C. Wang, G. Xie, Comparative study for convective heat transfer of counter-flow wavy double-layer microchannel heat sinks in staggered arrangement, Appl. Therm. Eng. 137 (2018) 228–237, https://doi.org/10.1016/j.applthermaleng.2018.03.089.
[24] S. Soleimanikutanaei, E. Ghasemisahebi, C.X. Lin, Numerical study of heat transfer enhancement using transverse microchannels in a heat sink, Int. J. Therm. Sci. 125 (2018) 89–100, https://doi.org/10.1016/j.ijthermalsci.2017.11.009.
[25] G. Xie, H. Shen, C.C. Wang, Parametric study on thermal performance of microchannel heat sinks with internal vertical Y-shaped bifurcations, Int. J. Heat Mass Transf. 90 (2015) 948–958, https://doi.org/10.1016/j.ijheatmasstransfer.2015.07.034.
[26] H. Shen, C.C. Wang, G. Xie, A parametric study on thermal performance of microchannel heat sinks with internally vertical bifurcations in laminar liquid flow, Int. J. Heat Mass Transf. 117 (2018) 487–497, https://doi.org/10.1016/j.ijheatmasstransfer.2017.10.025.
[27] B. Shen, H. Yan, B. Sunden, H. Xue, G. Xie, Forced convection and heat transfer of water-cooled microchannel heat sinks with various structured metal foams, Int. J. Heat Mass Transf. 113 (2017) 1043–1053, https://doi.org/10.1016/j.ijheatmasstransfer.2017.06.004.
[28] H. Shen, X. Liu, H. Yan, G. Xie, B. Sunden, Enhanced thermal performance of internal Y-shaped bifurcation microchannel heat sinks with metal foams, J. Therm. Sci. Eng. Appl. 10 (1) (2018), https://doi.org/10.1115/1.4036767.
[29] K.H. Cho, W.P. Chang, M.H. Kim, A numerical and experimental study to evaluate performance of vascularized cooling plates, Int. J. Heat Fluid Flow 32 (6) (2011) 1186–1198, https://doi.org/10.1016/j.ijheatfluidflow.2011.09.006.
[30] K.H. Cho, M.H. Kim, Transient thermal-fluid flow characteristics of vascular networks, Int. J. Heat Mass Transf. 55 (13–14) (2012) 3533–3540, https://doi.org/10.1016/j.ijheatmasstransfer.2012.02.075.
[31] Schubert, K., Pfeifer, P., Kraut, M., & Dittmeyer, R., (2011). Heat exchanger for rapidly heating and cooling fluids. WO2011134630. https://patents.google.com/patent/WO2011134630A1/en.
[32] F. Brighenti, N. Kamaruzaman, J.J. Brandner, Investigation of self-similar heat sinks for liquid cooled electronics, Appl. Therm. Eng. 59 (1–2) (2013) 725–732, https://doi.org/10.1016/j.applthermaleng.2013.01.001.
[33] N.B. Kamaruzaman, F. Brighenti, J.J. Brandner, A. Saat, Prediction of micro surface cooler performance for different rectangular type microchannels dimensions, Int. J. Heat Fluid Flow 44 (2013) 644–651, https://doi.org/10.1016/j.ijheatfluidflow.2013.09.005.
[34] W. Tang, L. Sun, H. Liu, G. Xie, Z. Mo, J. Tang, Improvement of flow distribution and heat transfer performance of a self-similarity heat sink with a modification to its structure, Appl. Therm. Eng. 121 (2017) 163–171, https://doi.org/10.1016/j.applthermaleng.2017.04.051.
[35] H.B. Yan, Q.C. Zhang, T.J. Lu, T. Kim, A lightweight X-type metallic lattice in single-phase forced convection, Int. J. Heat Mass Transf. 83 (2015) 273–283, https://doi.org/10.1016/j.ijheatmasstransfer.2014.11.061.
[36] X. Jin, B. Shen, H. Yan, B. Sunden, G. Xie, Comparative evaluations of thermofluidic characteristics of sandwich panels with X-lattice and pyramidal-lattice cores, Int. J. Heat Mass Transf. 127 (2018) 268–282, https://doi.org/10.1016/j.ijheatmasstransfer.2018.07.087.
[37] B. Shen, H. Yan, H. Xue, G. Xie, The effects of geometrical topology on fluid flow and thermal performance in Kagome cored sandwich panels, Appl. Therm. Eng. 142 (2018) 79–88, https://doi.org/10.1016/j.applthermaleng.2018.06.080.
[38] C. Pistoresi, Y. Fan, J. Aubril, L. Luo, Fluid flow characteristics of a multi-scale fluidic network, Chem. Eng. Process. Process Intensif. 123 (2018) 67–81, https://doi.org/10.1016/j.cep.2017.10.014.
[39] L. Luo, M. Wei, Y. Fan, G. Flamant, Heuristic shape optimization of baffled fluid distributor for uniform flow distribution, Chem. Eng. Sci. 123 (2015) 542–556, https://doi.org/10.1016/j.ces.2014.11.051.
[40] M. Wei, G. Boutin, Y. Fan, L. Luo, Numerical and experimental investigation on the realization of target flow distribution among parallel mini-channels, Chem. Eng. Res. Des. 113 (2016) 74–84, https://doi.org/10.1016/j.cherd.2016.06.026.
[41] R.J. Moffat, Describing the uncertainties in experimental results, Exp. Therm Fluid Sci. 1 (1) (1988) 3–17, https://doi.org/10.1016/0894-1777(88)90043-X.
[42] IAPWS (2016). Revised release on the IAPWS formulation 1995 for the thermodynamic properties of ordinary water substance for general and scientific use.
[43] S. Yang, W. Tao, Heat transfer, 3rd ed, Higher Education Press, Beijing, 1998.
[44] G.D. Xia, J. Jiang, J. Wang, Y.L. Zhai, D.D. Ma, Effects of different geometric structures on fluid flow and heat transfer performance in microchannel heat sinks, Int. J. Heat Mass Transf. 80 (2015) 439–447, https://doi.org/10.1016/j.ijheatmasstransfer.2014.08.095.
[45] X. Liu, J. Yu, Numerical study on performances of mini-channel heat sinks with non-uniform inlets, Appl. Therm. Eng. 93 (2016) 856–864, https://doi.org/10.1016/j.applthermaleng.2015.09.032.
[46] I.A. Ghani, N.A. Che Sidik, N. Kamaruzzaman, W. Jazair Yahya, O. Mahian, The effect of manifold zone parameters on hydrothermal performance of micro-channel heat sink: a review, Int. J. Heat Mass Transf. 109 (2017) 1143–1161, https://doi.org/10.1016/j.ijheatmasstransfer.2017.03.007.
[47] O.K. Siddiqui, S.M. Zubair, Efficient energy utilization through proper design of microchannel heat exchanger manifolds: a comprehensive review, Renew. Sustain. Energy Rev. 74 (2017) 969–1002, https://doi.org/10.1016/j.rser.2017.01.074.
[48] M. Medrano, M.O. Yilmaz, M. Nogués, I. Martorell, J. Roca, L.F. Cabeza, Experimental evaluation of commercial heat exchangers for use as PCM thermal storage systems, Appl. Energy 86 (10) (2009) 2047–2055, https://doi.org/10.1016/j.apenergy.2009.01.014.
[49] D. Tarlet, Y. Fan, S. Roux, L. Luo, Entropy generation analysis of a mini heat exchanger for heat transfer intensification, Exp. Therm Fluid Sci. 53 (2014) 119–126, https://doi.org/10.1016/j.expthermflusci.2013.11.016.
[50] K. Merlin, J. Soto, D. Delaunay, L. Traonvouez, Industrial waste heat recovery using an enhanced conductivity latent heat thermal energy storage, Appl. Energy 183 (2016) 491–503, https://doi.org/10.1016/j.apenergy.2016.09.007.